AGU PUBLICATIONS

Water Resources Research

RESEARCH ARTICLE
10.1002/2016WR019672

An analytical test case for snow models

Martyn P. Clark[1], Bart Nijssen[2], and Charles H. Luce[3]

[1]National Center for Atmospheric Research, Boulder, Colorado, USA, [2]Department of Civil and Environmental Engineering, University of Washington, Seattle, Washington, USA, [3]United States Forest Service, Boise, Idaho, USA

Key Points:
- We present an analytical test case to evaluate physically motivated snow models
- The analytical solutions evaluate the coupling of the energy and mass balance as well as unsaturated flow of water through snow
- The intended use of the test cases is to evaluate the impact of different numerical approximations

Correspondence to:
M. P. Clark,
mclark@ucar.edu

Citation:
Clark, M. P., B. Nijssen, and C. H. Luce (2017), An analytical test case for snow models, *Water Resour. Res.*, *53*, 909–922, doi:10.1002/2016WR019672.

Received 18 AUG 2016
Accepted 28 NOV 2016
Accepted article online 17 DEC 2016
Published online 31 JAN 2017

Abstract This paper develops general analytical solutions for examples of water movement through snow and compares the derived analytical solutions to numerical simulations from a coupled energy and mass balance model. The intended use of the test cases is to evaluate the impact of different numerical approximations, especially different vertical discretization strategies and different time stepping schemes. The analytical solutions provide both outflow from the snowpack, as well as vertical profiles of temperature and volumetric liquid water content at different times throughout the analysis period. The derived analytical solutions have close correspondence with model simulations in most cases. The most pronounced differences between the numerical simulations and the analytical solutions are for the fresh snow test case, where the numerical simulations predict earlier arrival of snowpack outflow. The analytical solutions provide a useful test case for physically motivated snow models because the solutions can be used to evaluate the coupling of hydrology and thermodynamics as well as the unsaturated flow of water through porous media.

1. Introduction

Improving numerical models of Earth System processes requires a systematic and comprehensive strategy for model evaluation. The four components of model evaluation defined by *Clark et al*. [2015a] are: (1) Synthetic test cases to check the equations are implemented correctly and that the numerical approximations are reasonable [*Celia et al*., 1990; *Wigmosta and Lettenmaier*, 1999; *Hansson et al*., 2004; *Kurylyk et al*., 2014; *Maxwell et al*., 2014]; (2) Process-level diagnostics to evaluate the realism of model representations of nature, isolating and evaluating individual model components wherever possible [*Stöckli et al*., 2008; *Yilmaz et al*., 2008; *Clark et al*., 2011; *Lawrence et al*., 2011; *Niu et al*., 2011; *Yang et al*., 2011; *Essery et al*., 2013]; (3) Analysis of the interplay between predictive accuracy and model complexity, to identify the information gains from more detailed process representations [*Jakeman and Hornberger*, 1993; *Boone and Wetzel*, 1996; *Desborough*, 1999; *Boone and Etchevers*, 2001; *Hogue et al*., 2006; *Magnusson et al*., 2015]; and (4) Formal statistical benchmarking to evaluate the extent to which models use the available information [*Abramowitz et al*., 2008; *Abramowitz*, 2012; *Best et al*., 2015; *Nearing et al*., 2016]. Taken together, such a comprehensive and systematic model evaluation strategy enables model development groups to reduce model errors, improve model fidelity, and identify priorities for future model development.

Synthetic test cases are a fundamental component of any model evaluation strategy. After all, synthetic test cases provide information on the accuracy of the numerical approximations, and such test cases are hence critical to understand how numerical approximations impact capabilities for process evaluation and hypothesis testing [*Clark and Kavetski*, 2010; *Kavetski and Clark*, 2010, 2011]. This is especially true in the land component of Earth System Models, where model development groups often adopt a myriad of numerical simplifications to accomplish global simulations [*Lawrence et al*., 2011; *Niu et al*., 2011]. Common numerical simplifications in snow models include decoupling the conservation equations for energy and mass, adopting non-iterative numerical solutions for the conservation equations, configuring models with coarse vertical resolution, and ignoring the propagation of water through the snowpack [*Essery et al*., 2013]. Synthetic test cases are hence the logical next step beyond code verification to ensure that the intent behind a given numerical solution is actually accomplished.

The purpose of this paper is to fully develop test cases for the examples of water movement through snow that were introduced by *Colbeck* [1976]. Colbeck considered a constant rain rate applied at the top of a 1 m

snowpack for 3 h for different initial snow conditions: (1) ripe snow (temperature 0°C and grain size 2mm); (2) refrozen snow (temperature −5°C and grain size 2 mm); and (3) fresh snow (temperature −5°C and grain size 0.2 mm). The colder initial temperatures for refrozen and fresh snow require that both a heat deficit and a residual saturation deficit are satisfied before flow occurs; the smaller grain size for fresh snow substantially reduces the permeability of the snowpack and slows the flow of water. Colbeck's examples provide a useful test case for snow models because they evaluate the coupling of hydrology and thermodynamics (i.e., the freezing of water onto the snow grains necessary to supply sufficient latent heat to raise the snow temperature to 0°C), as well as providing a means to evaluate the unsaturated flow of water through porous media. Because of the nonlinearities inherent in the unsaturated flow case and the threshold behavior of a wetting front, these test cases offer a strong test of numerical techniques using local derivatives. These test cases are intended to be general and useful to test a suite of physically motivated snow models [*Luce et al*., 1999; *Marks et al*., 1999; *Bartelt and Lehning*, 2002; *Vionnet et al*., 2012].

The specific contribution of this paper is to develop general analytical solutions for Colbeck's examples of water movement through snow, and compare the derived analytical solutions to numerical simulations from a coupled energy and mass balance model. Colbeck's examples were previously used in the development of the SNTHERM model, but with large discrepancies between Colbeck's calculations and the SNTHERM simulations [*Jordan*, 1991]. R. Jordan (1991) explained these discrepancies based on personal communication with Colbeck: "Colbeck indicated that he used a graphic procedure and that the numerical solutions should be more accurate." [*Jordan*, 1991, p. 34]. Put simply, Colbeck's calculations were not sufficiently accurate to provide a robust test case for snow models, and there is a need to fully develop analytical solutions for Colbeck's examples so that they can be used as part of a comprehensive model evaluation system.

As will be shown below, Colbeck's examples have exact analytical solutions. In fact, the analytical solutions to Colbeck's examples are very similar to the numerical model simulations from SNTHERM presented in *Jordan* [1991], suggesting that *Jordan*'s confidence in her numerical model was justified. However, it is important to note here that Jordan's acceptance of SNTHERM was gained by intuition instead of model evaluation, since Colbeck's graphically based calculations were deemed less accurate than the numerical simulations. We address this issue by developing analytical solutions for Colbeck's examples. The analytical solutions developed in this paper go beyond what was presented by *Colbeck* [1976] and used by *Jordan* [1991]–the solutions provide information on both outflow from the snowpack as well as information on vertical profiles of temperature and volumetric liquid water content at different times throughout the analysis period. These analytical solutions to Colbeck's water flow examples provide new capabilities to test the numerical implementation of physically motivated snow models.

2. State and Flux Equations

2.1. Conservation Equations

The model presented here is intended to be very general, representing the equations used in most physically motivated snow models [*Clark et al*., 2015b, 2015d].

We represent the snowpack as a mixture of ice, liquid water, and air, i.e.,

$$\sum_k \theta_k = 1 \tag{1}$$

where θ_k is the volumetric fraction of the k-th constituent (k=*ice*, *liq*, *air*), and we define porosity ϕ as the space between ice crystals

$$\phi = 1 - \theta_{ice} \tag{2}$$

The volumetric heat capacity is

$$C_p = \sum_k \rho_k c_k \theta_k \tag{3}$$

where c_k (J kg^{-1} K^{-1}), ρ_k (kg m^{-3}) and θ_k (-) define the specific heat, the intrinsic density, and the volumetric fraction of the k-th constituent, respectively, with ρ_{liq}=1000 kg m^{-3}, ρ_{ice}=917 kg m^{-3}, ρ_{air} depending on meteorological conditions, and c_{ice}=2114 J kg^{-1} K^{-1}, c_{liq}=4181 J kg^{-1} K^{-1}, and c_{air}=1005 J kg^{-1} K^{-1}.

The conservation equations for energy and mass are defined using the state variables of temperature T (K) and total volumetric water content Θ_m, with $\Theta_m = \theta_{liq} + \rho_{ice}\theta_{ice}/\rho_{liq}$. The state equations are [*Clark et al.*, 2015d,c]

$$C_p \frac{\partial T}{\partial t} - \rho_{ice} L_{fus} \left(\frac{\partial \theta_{ice}}{\partial t} \right)_{mf} = -\frac{\partial F}{\partial z} \tag{4}$$

$$\frac{\partial \Theta_m}{\partial t} = -\frac{\partial q_{liq}}{\partial z} \tag{5}$$

where C_p (J m^{-3} K^{-1}) is the volumetric heat capacity, L_{fus} (J kg^{-1}) is the latent heat of fusion, F (J m^{-2} s^{-1}) and q_{liq} (m s^{-1}) are the vertical fluxes of energy and liquid water, and z (m) and t (s) are the coordinates for depth and time. The subscript *mf* in equation (4) denotes that we restrict attention to the change in ice content associated with melting and freezing, i.e., that densification is handled separately. The partitioning of Θ_m into volumetric liquid water content θ_{liq} and volumetric ice content θ_{ice} is defined as a function of temperature (see section 2.2).

In equation (5), the time evolution of total volumetric water content only depends on the flux of liquid water (i.e., we ignore snowfall and sublimation at the upper boundary of the snowpack, both of which are handled separately because they change the structure of the snow domain). That is, equation (5) assumes that ice is immobile. The change in phase associated with melting and freezing is implicit in equation (5) since $\Theta_m = \theta_{liq} + \rho_{ice}\theta_{ice}/\rho_{liq}$.

2.2. Closure Relations

The volumetric fraction of liquid water θ_{liq} is defined as a function of total volumetric water content and temperature as [*Clark et al.*, 2015d]

$$\theta_{liq}(\Theta_m, T) = \frac{\Theta_m}{1 + [\varpi(T_{frz} - T)]^2} \qquad T \leq T_{frz} \tag{6}$$

The volumetric ice content θ_{ice} is then obtained using $\Theta_m = \theta_{liq} + \rho_{ice}\theta_{ice}/\rho_{liq}$. In equation (6) T_{frz} (K) is the freezing point of pure water and ϖ (K^{-1}) is a scaling parameter. Equation (6) defines a smoothed step function over a small temperature interval below T_{frz}, ranging from zero to Θ_m at T_{frz}. The parameter ϖ defines the degree of smoothing ($\varpi = 50$ defines a function that is visually indistinguishable from a step function over a typical diurnal temperature range).

Analogous to *Colbeck* [1976], the vertical liquid flux is related to the volume fraction of liquid water as

$$q_{liq} = kS^n \tag{7}$$

where k (m s^{-1}) is the saturated hydraulic conductivity, S is the relative saturation, and n is an exponent, with k and S given as [*Colbeck*, 1976; *Colbeck and Anderson*, 1982]

$$k = \frac{\rho_{liq} g}{\mu} \kappa \tag{8}$$

$$S = \frac{\theta_{liq} - \theta_r}{\phi - \theta_r} \tag{9}$$

With θ_r residual volumetric liquid water content, κ permeability (m^2), g acceleration due to gravity (m s^{-2}), $g = 9.81$ m s^{-2}, μ dynamic viscosity (kg m^{-1} s^{-1}), $\mu = 1.781 \times 10^{-3}$ kg m^{-1} s^{-1}.

The energy fluxes on the right-hand-side of equation (4) are set to zero for Colbeck's water flow examples, and are not discussed here. The reader is referred to *Clark et al.* [2015c] for a review of commonly used parameterizations for energy fluxes.

3. An Analytical Test Case for Snow Models

The analytical test case we develop here derives from Colbeck's theory of infiltration into dry snow [*Colbeck*, 1972, 1976]. In the next sections, we first present the theory of water movement in dry snow, and then the analytical solutions.

3.1. Theory

3.1.1. Downward Propagation of the Wetting Front

Colbeck [1976] defines three requirements that must be met before the wetting front can propagate past any depth:

1. Infiltrating water must be frozen onto the snow grains to supply sufficient latent heat to raise the snow to 0°C;
2. Infiltrating water must exceed the residual water requirement, i.e., immobile water held under tension; and
3. The water content immediately below the wetting front must be raised to the level of saturation at the wetting front.

The water required to satisfy the thermal requirements can be calculated from the conservation equation for energy. Given dry snow, ignoring the heat capacity of air, (i.e., $C_p = \rho_{ice} c_{ice} \theta_{ice}$), given a vertical energy flux of zero, and noting that $\rho_{ice} \partial\theta_{ice}/\partial t = -\rho_{liq} \partial\theta_{liq}/\partial t$, equation (4) can be rearranged to define the amount of liquid water that must be frozen to satisfy thermal requirements

$$\theta_f = \frac{\rho_{ice} c_{ice}}{\rho_{liq} L_{fus}} (\phi - 1) \Delta T \tag{10}$$

where $\Delta T = T - T_{frz}$ and $\rho_{ice} c_{ice} / \rho_{liq} L_{fus} \approx 0.0058\ \mathrm{K}^{-1}$.

The residual, or irreducible water requirement is a function of porosity

$$\theta_r = S_{wi} \phi \tag{11}$$

where S_{wi} (-) is the fraction of pore space that must be filled before flow begins (*Colbeck* [1976] gives $S_{wi} \approx 0.07$ based on lysimeter experiments, and this value is also adopted here). Note that since S_{wi} is much greater than the constant $\rho_{ice} c_{ice} / \rho_{liq} L_{fus}$ used in equation (10), in snowpacks where liquid water is likely to be introduced the amount of water required to satisfy the residual water content is typically much greater than the amount of liquid water that must be frozen to satisfy thermal requirements [*Colbeck*, 1976].

Once the thermal and irreducible liquid water requirements are satisfied, the downward propagation of the wetting front is dictated by the third requirement that the relative saturation immediately below the front be raised to the relative saturation at the wetting front S_w(-). We can then use equation (7) to solve for S_w

$$S_w = \left(\frac{q_w}{k}\right)^{1/n} \tag{12}$$

where q_w (m s^{-1}) is the flux at the wetting front. The downward propagation of the wetting front can then be calculated by combining equations (10) and (12) as

$$\frac{dz_w}{dt} = \frac{q_w}{\theta_f + (\theta_w - \theta_0)} \tag{13}$$

where z_w is the depth of the wetting front, θ_w is the volumetric liquid water content necessary to sustain the level of flux at the wetting front, i.e., $\theta_w = \theta_r + (\phi - \theta_r) S_w$, and θ_0 is the initial volumetric liquid water content.

3.1.2. Gravity Drainage Above the Wetting Front

The method of characteristics can be used to calculate vertical profiles of the volumetric liquid water content at any time during the analysis period as well as time series of the water flux at any point within the snowpack (e.g., snowpack outflow). The method of characteristics has been widely used for unsaturated flow, saturated flow, and overland flow problems [*Sisson et al.*, 1980; *Beven*, 1982; *Charbeneau*, 1984; *Luce and Cundy*, 1992; *Wigmosta and Lettenmaier*, 1999], all of which have some similarities to the solutions presented here.

Once the heat deficits have been satisfied, and assuming that the liquid water will not re-freeze (arguably a reasonable assumption during rain-on-snow events), the conservation equation for mass, equation (5), can be rewritten as

$$\frac{\partial \theta_{liq}}{\partial t} = -\frac{\partial q_{liq}}{\partial z} \tag{14}$$

Equation (14) can be solved using the method of characteristics to convert the partial differential equation into an ordinary differential equation [*Courant and Hilbert*, 1962]. First we rearrange and apply the chain rule to the depth derivative, noting that q_{liq} only depends on θ_{liq}

$$\frac{\partial \theta_{liq}}{\partial t} + \frac{dq_{liq}}{d\theta_{liq}} \frac{\partial \theta_{liq}}{\partial z} = 0 \tag{15}$$

where differentiating equation (7) with respect to the volumetric liquid water content θ_{liq} gives

$$\frac{dq_{liq}}{d\theta_{liq}} = \frac{n}{\phi - \theta_r} k \left(\frac{\theta_{liq} - \theta_r}{\phi - \theta_r} \right)^{n-1} \tag{16}$$

We next define a parametric curve, $z(p)$, $t(p)$, called a characteristic curve, along which the solution is given as an ordinary differential equation. By the chain rule, the total derivative of θ_{liq} with respect to p is

$$\frac{d\theta_{liq}}{dp} = \frac{\partial \theta_{liq}}{\partial t} \frac{dt}{dp} + \frac{\partial \theta_{liq}}{\partial z} \frac{dz}{dp} \tag{17}$$

so if we chose our parametric curve with

$$\frac{dt}{dp} = 1 \tag{18}$$

and

$$\frac{dz}{dp} = \frac{dq_{liq}}{d\theta_{liq}} \tag{19}$$

then

$$\frac{d\theta_{liq}}{dp} = \frac{\partial \theta_{liq}}{\partial t} + \frac{dq_{liq}}{d\theta_{liq}} \frac{\partial \theta_{liq}}{\partial z} = 0 \tag{20}$$

meaning that the curves defined by equations (18) and (19) are curves of constant θ_{liq} and consequently constant q_{liq}. Taking the ratio of equations (18) and (19), we can calculate the slope of these curves on the $z-t$ plane

$$\left. \frac{dz}{dt} \right|_{\theta_{liq}=const} = \frac{dz}{dp} \frac{dp}{dt} = \frac{dq_{liq}}{d\theta_{liq}} \frac{dp}{dt} \tag{21}$$

and noting from equation (18) that $dp/dt = 1$ and making use of equation (16)

$$\left. \frac{dz}{dt} \right|_{\theta_{liq}=const} = \frac{nk}{\phi - \theta_r} \left(\frac{\theta_{liq} - \theta_r}{\phi - \theta_r} \right)^{n-1} \tag{22}$$

An equivalent solution for the constant flux can be derived

$$\left. \frac{dz}{dt} \right|_{q_{liq}=const} = \frac{nk}{\phi - \theta_r} \left(\frac{q_{liq}}{k} \right)^{(n-1)/n} \tag{23}$$

Equations (22) and (23) form the basis of the analytical solutions for water movement through snow described in the next section.

3.2. Analytical Solutions

The following sections provide examples for both the full duration case, where the snowpack reaches steady state during the simulation period, and the partial duration case where the snowpack does not reach steady state.

3.2.1. The Full Duration Case

The outflow hydrograph for situations where the snowpack reaches steady state is illustrated in Figure 1, using the example from *Colbeck* [1976] for refrozen snow (Table 1), where constant rain rate of 0.01 mm s^{-1} is applied at the top of a 1 m snowpack for 3 h. Equations (13) and (23) are used for the rising hydrograph to calculate the time when the wetting and drying fronts reach the bottom of the snowpack, t_{wb} and t_{db}

$$t_{wb} = t_0 + z_b \left(\frac{dz_w}{dt} \right)^{-1} \tag{24}$$

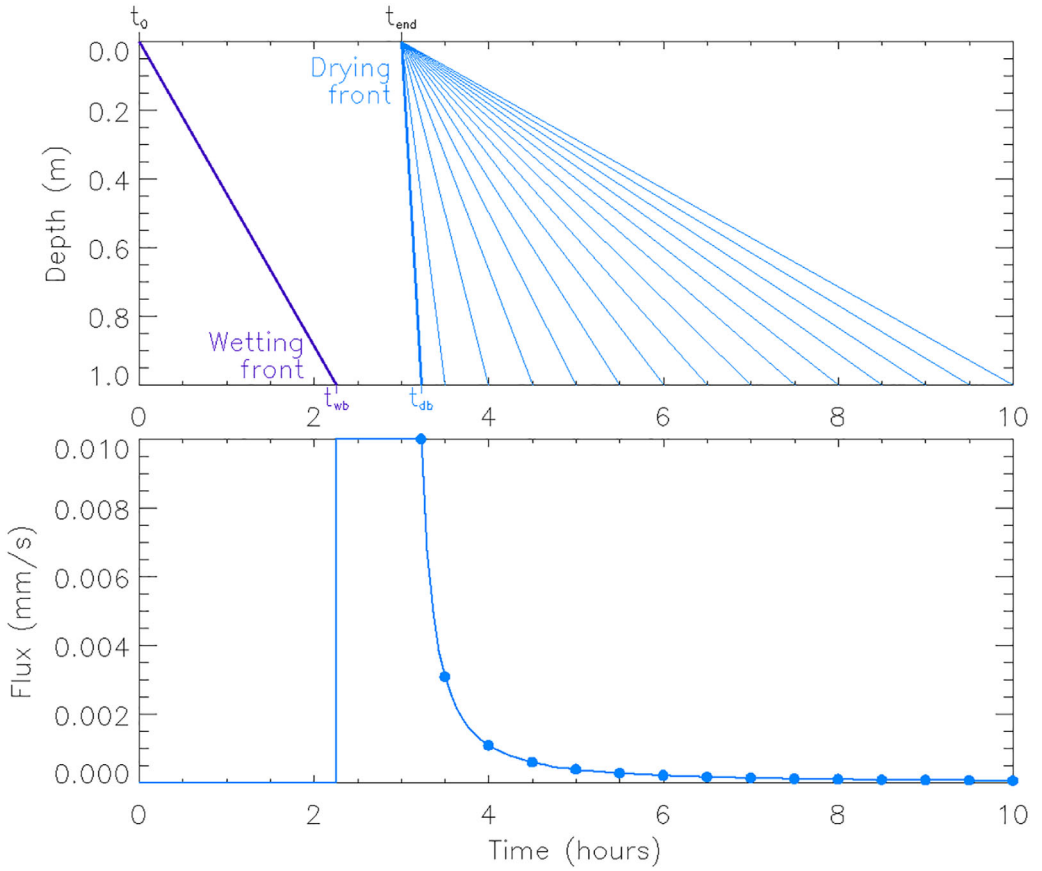

Figure 1. Water movement through a 1 m deep snowpack for the "refrozen snow" test case (Table 1), where a constant rain rate of 0.01 mm s^{-1} is applied at the top of a 1 m snowpack for 3 h. In this test case the snowpack reaches steady state. The top plot illustrates the downward propagation of the wetting front, the drying front, and characteristic lines with constant volumetric water content and liquid flux. The bottom plot illustrates the fluxes at the bottom of the snowpack.

$$t_{db} = t_{end} + z_b \left(\left. \frac{dz}{dt} \right|_{q_{rain}} \right)^{-1} \tag{25}$$

where equation (25) is evaluated at $q_{liq} = q_{rain}$. Here z_b (m) is the depth at the bottom of the snowpack, and t_{wb} and t_{db} are the times when the wetting and drying fronts reach the bottom of the snowpack, respectively (Figure 1). We use the term "drying front" to denote the depth of maximum saturation after the rain has stopped, defined at a given time $t - t_{end}$ using the characteristic from equation (23) with $q_{liq} = q_{rain}$. The snowpack reaches steady state for the period that $t_{wb} < t < t_{db}$ (note that $t_{wb} > t_{db}$ defines the partial duration case considered in the next section). For the rising hydrograph $q_{liq}(z_b, t) = 0$ when $t \leq t_{wb}$ and during steady state $q_{liq}(z_b, t) = q_{rain}$ when $t_{wb} < t < t_{db}$.

Table 1. Initial Snow Conditions for the Water Flow Examples Presented by *Colbeck* [1976]

	Ripe Snow	Refrozen Snow	Fresh Snow
Snow density (kg m^{-3})	300	300	300
Temperature (°C)	0	−5	−5
Grain size (mm)	2	2	0.2
Permeability (m^2)[a]	2.967×10^{-8}	2.967×10^{-8}	2.967×10^{-10}
Porosity[b]	0.728	0.673	0.673
Vol. liquid water	0.051	0.000	0.000
Vol. ice content	0.272	0.327	0.327

[a]Permeability was estimated using the *Shimizu* [1970] empirical formula, $\kappa/d^2 = 0.077\exp(-7.8\rho_s/\rho_{liq})$, where d (m) is the grain size.
[b]Porosity is estimated given $\rho_s = \theta_{ice}\rho_{ice} + \theta_{liq}\rho_{liq}$ with $\theta_{ice} = 1 - \phi$. For ripe snow the initial volumetric liquid water content is $\theta_{liq} = \theta_r = S_{wi}\phi$, so $\rho_s = (1-\phi)\rho_{ice} + S_{wi}\phi\rho_{liq}$ (with $S_{wi} = 0.07$); for refrozen and fresh snow the initial liquid water content $\theta_{liq} = 0$, hence $\rho_s = (1-\phi)\rho_{ice}$.

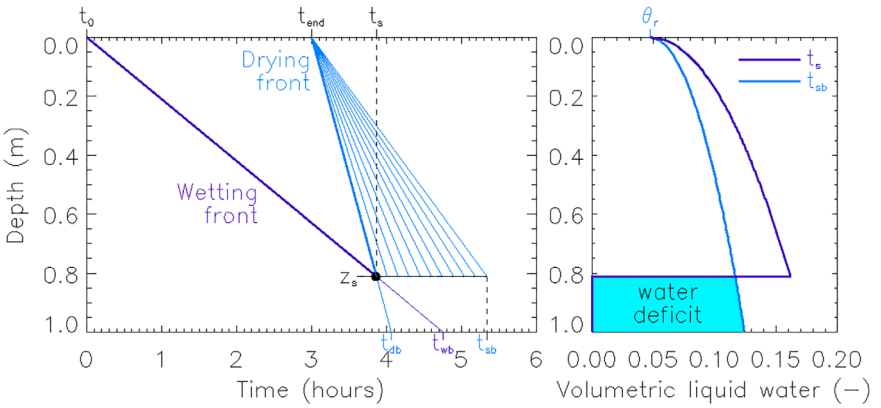

Figure 2. Water movement through a 1 m deep snowpack for the "fresh snow" test case (Table 1), where a constant rain rate of 0.01 mm s^{-1} is applied at the top of a 1 m snowpack for 3 h. In this test case the snowpack does not reach steady state. The left plot illustrates the downward propagation of the wetting front and the drying front, and the space-time location of the kinematic shock (z_s, t_s). The characteristic lines, which reach depth z_s after time t_s, define time varying forcing at depth z_s. The right plot illustrates the vertical profiles of volumetric liquid water at times t_s and the (currently unknown) time t_{sb} when the wetting front ultimately reaches the bottom of the snowpack. The vertical integration of the volumetric liquid water at time t_{sb} defines the water deficit that must be satisfied by the volume flux across the boundary z_s.

The falling hydrograph is calculated based on the theory that the relative saturation at the surface instantly drops to zero when the rain stops, that is, $S(z=0,\ t=t_{end})=0$. Because the relative saturation and the flux are uniquely related through equation (7), the instantaneous drop in S means that an infinite number of characteristic lines intersect the point $(z=0,\ t=t_{end})$ with slope z/t, which is less than the slope of the characteristic associated with the drying front (Figure 1). For $t > t_{db}$ the celerity of a given characteristic is simply $dz/dt=z/(t-t_{end})$. The outflow flux at time t can then be calculated by solving equation (23) for q_{liq} at depth $z=z_b$, giving the falling hydrograph for $t > t_{db}$ as

$$q_{liq}(z,t)=k\left(\frac{z(\phi-\theta_r)}{(t-t_{end})nk}\right)^{n/(n-1)} \tag{26}$$

The characteristic lines in Figure 1 also define the vertical profile in volumetric liquid water content at time t. For example, given $dz/dt=z/(t-t_{end})$, the vertical profile of θ_{liq} can be calculated by solving equation (22) for θ_{liq} at time $t=t_{db}$ as

$$\theta_{liq}(z,\ t)=\theta_r+(\phi-\theta_r)\left(\frac{z(\phi-\theta_r)}{(t-t_{end})nk}\right)^{1/(n-1)} \tag{27}$$

Equation (27) is important for the solution of the partial duration case described next.

3.2.3. The Partial Duration Case

Figure 2 illustrates the propagation of water through snow for the case that the snowpack does not reach steady state conditions, using the example from *Colbeck* [1976] for fresh snow (Table 1). As in the previous example a constant rain rate of 0.01 mm s^{-1} is applied at the top of a 1 m snowpack for 3 h. In this example $t_{db} < t_{wb}$, meaning that the snowpack never reaches steady state and that the drying front overtakes the wetting front before the wetting front reaches the bottom of the snowpack, creating a kinematic shock at point (z_s, t_s). Given that the wetting and drying characteristics intersect at time t_s, we can combine equations (24) and (25)

$$t_0+z_s\left(\frac{dz_w}{dz}\right)^{-1}=t_{end}+z_s\left(\frac{dz}{dz}\bigg|_{q_{rain}}\right)^{-1} \tag{28}$$

to solve for the depth of the shock z_s (m)

$$z_s=\frac{t_{end}-t_0}{\left(\frac{dz}{dt}|_{q_{rain}}\right)^{-1}-\left(\frac{dz_w}{dt}\right)^{-1}} \tag{29}$$

with the time of the shock $t_s=t_0+z_s(dz_w/dt)^{-1}$ (see Figure 2, top left).

The kinematic shock results in time varying inputs to the wetting front (Figure 2, left) that are required to satisfy the thermal and liquid requirements defined in equation (13). Because the downward propagation of the wetting front is dictated by the requirement that the relative saturation immediately below the front S_w be raised to the level to satisfy the flux at the wetting front, the time varying inputs create time varying water requirements.

The problem is solved as follows. Consider for the moment that we know the time that the merged shock t_{sm} reaches a given depth z_{sm}, where $t_{sm} > t_s$ and $z_{sm} > z_s$. Using equation (27) to define the vertical profile of θ_{liq} at time t_{sm} (see the right plot in Figure 2, for the case $z{=}z_b$), the volume flux needed to satisfy thermal and liquid requirements can be obtained by integrating the θ_{liq} profile from z_s to z_{sm}, providing the equality

$$\int_{t_s}^{t_{sm}} q_{liq}(z_s,\, t)\, dt = \int_{z_s}^{z_{sm}} \left[\theta_{liq}(z,\, t_{sm}) + \theta_f\right] dz \qquad z > z_s, \quad t > t_s \tag{30}$$

That is, the volume flux across the boundary z_s over the time t_s to t_{sm} must match the thermal and liquid deficits over the depth z_s to z_{sm} at time t_{sm}. The mass balance in equation (30) does not just apply at the bottom of the snowpack (as illustrated in Figure 2), but is true for all $z > z_s$. The use of general limits of integration, t_{sm} and z_{sm} in equation (30) enables tracing the shock analytically in place of the approximate graphical solution previously used by *Colbeck* [1976].

Equation (30) provides the basis to solve for the temporal progression of the merged shock t_{sm}. Combining equations (26), (27), and (30),

$$\int_{t_s}^{t_{sm}} k\left(\frac{z_s(\phi-\theta_r)}{(t-t_{end})nk}\right)^{n/(n-1)} dt = \int_{z_s}^{z_{sm}} \left[\theta_f + \theta_r + (\phi-\theta_r)\left(\frac{z(\phi-\theta_r)}{(t_{sm}-t_{end})nk}\right)^{1/(n-1)}\right] dz \tag{31}$$

and defining constants as

$$a_0 = \theta_f + \theta_r,$$

$$b_0 = (\phi-\theta_r)\left(\frac{(\phi-\theta_r)}{nk}\right)^{1/(n-1)}, \text{ and}$$

$$c_0 = k\left(\frac{z_s(\phi-\theta_r)}{nk}\right)^{n/(n-1)},$$

we find that the merged shock at time t_{sm} is

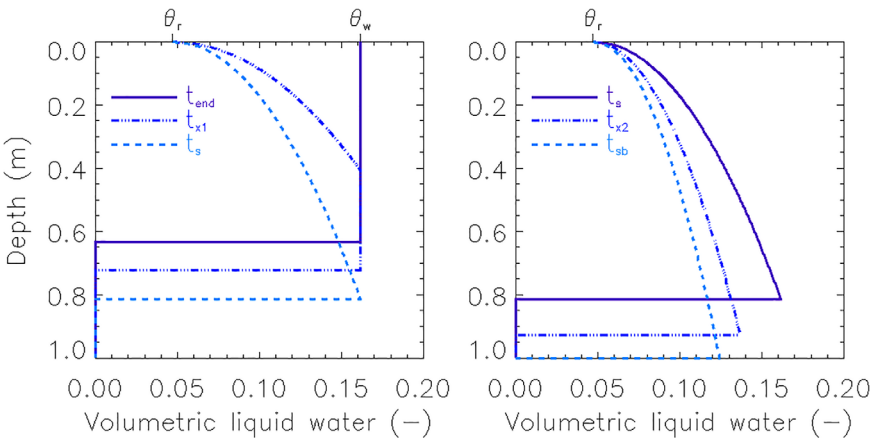

Figure 3. Vertical profiles of volumetric liquid water for the fresh snow test case. The left plot illustrates profiles for times from the end of the rainfall (t_{end}) until the time of the kinematic shock (t_s), and the right plot illustrates profiles from the time of the kinematic shock until the time the shock reaches the bottom of the snowpack (t_{sb}). In the left plot $t_{x1} = (t_{end} + t_s)/2$ and in the right plot $t_{x2} = (t_s + t_{sb})/2$.

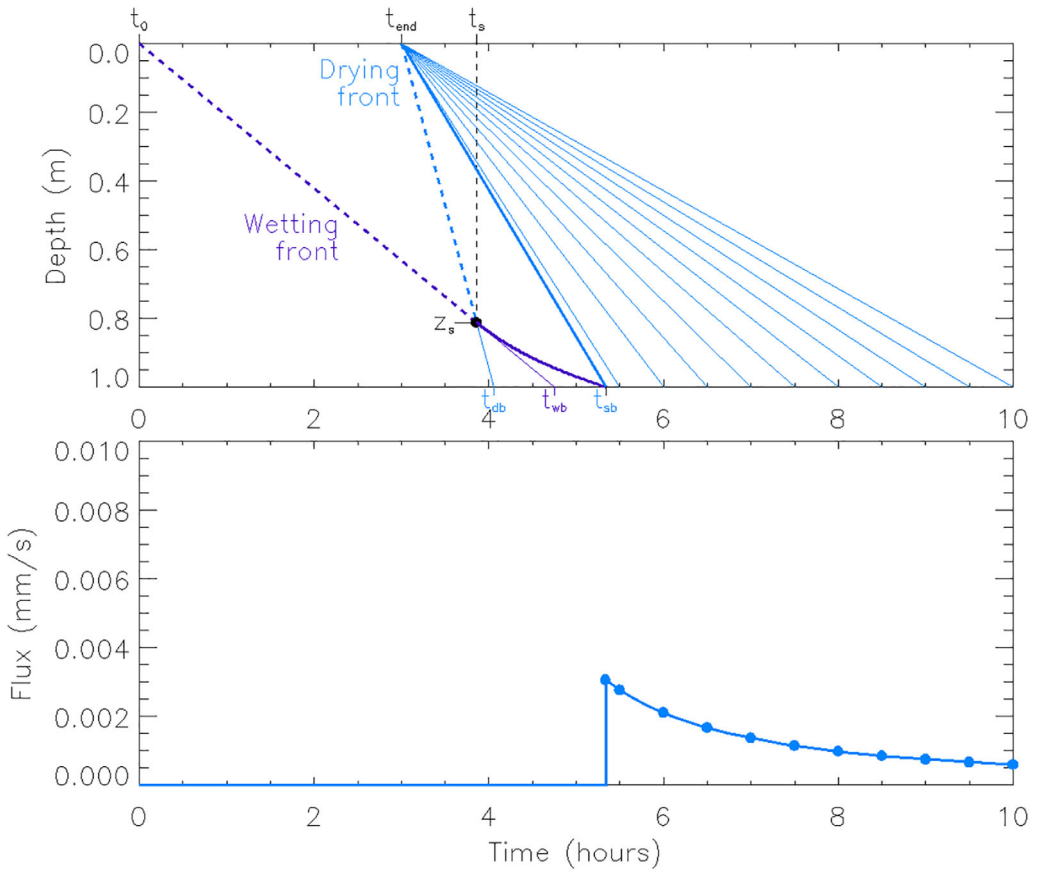

Figure 4. Water movement through a 1 m deep snowpack for the "fresh snow" test case (Table 1), where the snowpack does not reach steady state. The top plot illustrates the downward propagation of the wetting front, the drying front, the space-time location of the kinematic shock (z_s, t_s), and characteristic lines with constant volumetric water content and liquid flux. The bottom plot illustrates the fluxes at the bottom of the snowpack.

$$t_{sm}(z) = \left[\frac{c_0(1-n)(t_s - t_{end})^{1/(1-n)} + a_0(z - z_s)}{c_0(1-n) - b_0\left(\frac{n-1}{n}\right)\left[z^{n/(n-1)} - z_s^{n/(n-1)}\right]}\right]^{1-n} \qquad z > z_s \tag{32}$$

The merged shock then reaches the bottom of the snowpack in the partial duration case at time $t_{sb} = t_{sm}(z = z_b)$. As with the steady state situation, the falling hydrograph can then be calculated for all times after t_{sb} by calculating the celerity of each characteristic $dz/dt = z_b/(t - t_{end})$ and by solving equation (23) for q_{liq} at depth z_b.

Figures 3 and 4 use these analytical solutions to illustrate features of the partial duration test case. Figure 3 illustrates that the piston-like wetting front at the end of the rain period t_{end} exhibits drying from above (left plot), until the time of the kinematic shock t_s when the entire vertical profile is drier than the water content at the wetting front. After the kinematic shock the progression of the wetting front slows considerably (Figure 3, right) because of reductions in the magnitude of the fluxes at the boundary z_s (illustrated in Figure 2). The final result, shown in Figure 4, is that the peak snowpack outflow is substantially lower than the rain rate, and drying of the snowpack causes flow to recede immediately. These features provide the ingredients for a challenging test case for numerical models, as described in the next section.

4. Model Simulations

The conservation equations and closure relations described in section 2 are implemented in the Structure for Unifying Multiple Modeling Alternatives (SUMMA) hydrologic modeling system [*Clark et al.*, 2015b, 2015c, 2015d]. The conservation equations are solved by vertically discretizing the snowpack into 100 layers

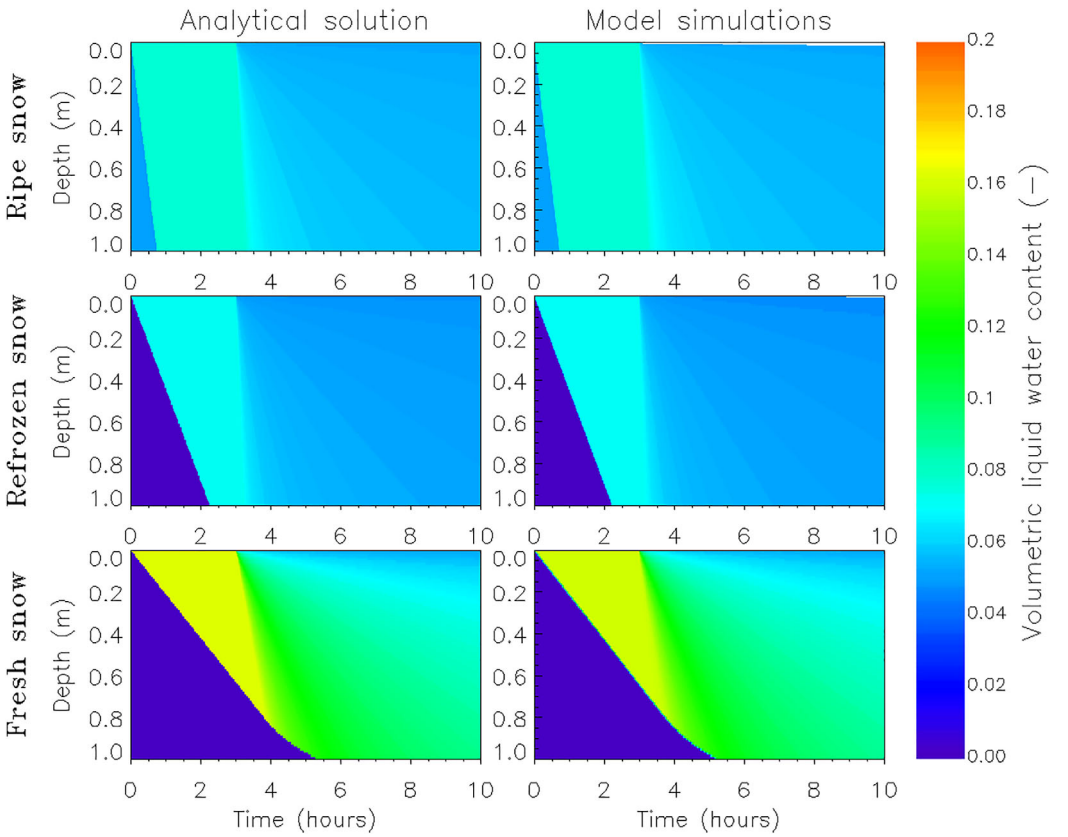

Figure 5. Contour plots of the volumetric liquid water content from the analytical solution and the numerical simulations (left plots and right plots respectively), for the ripe snow test case (top row), the refrozen snow test case (middle row), and the fresh snow test case (bottom row).

and using a fully implicit Newton-Raphson scheme for model time stepping. *Clark et al.* [2015d] provide specific details on the model implementation.

Figures 5–7 illustrate comparisons between the numerical simulations and model simulations. The contour plots in Figure 5 illustrate that the numerical simulations and analytical solutions are very similar for all three test cases, building confidence in the numerical model implementation. The vertical profiles of volumetric liquid water for specific times (Figure 6) illustrate that the model simulations are smoother than the analytical solutions. In Figure 7, the simulations show that some water moves ahead of the wetting front (bottom

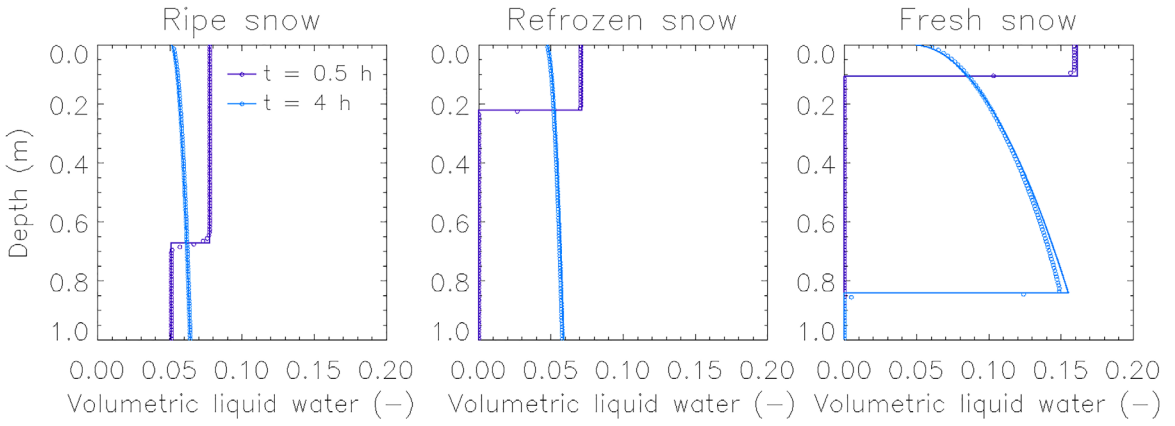

Figure 6. Vertical profiles of volumetric liquid water content from numerical simulations (small circles) and analytical solutions (solid lines). Results are shown for 0.5 h and 4 h since the beginning of the simulation. The left plot shows results for the ripe snow test case, the middle plot for the refrozen snow test case, and the right plot shows results for the fresh snow test case.

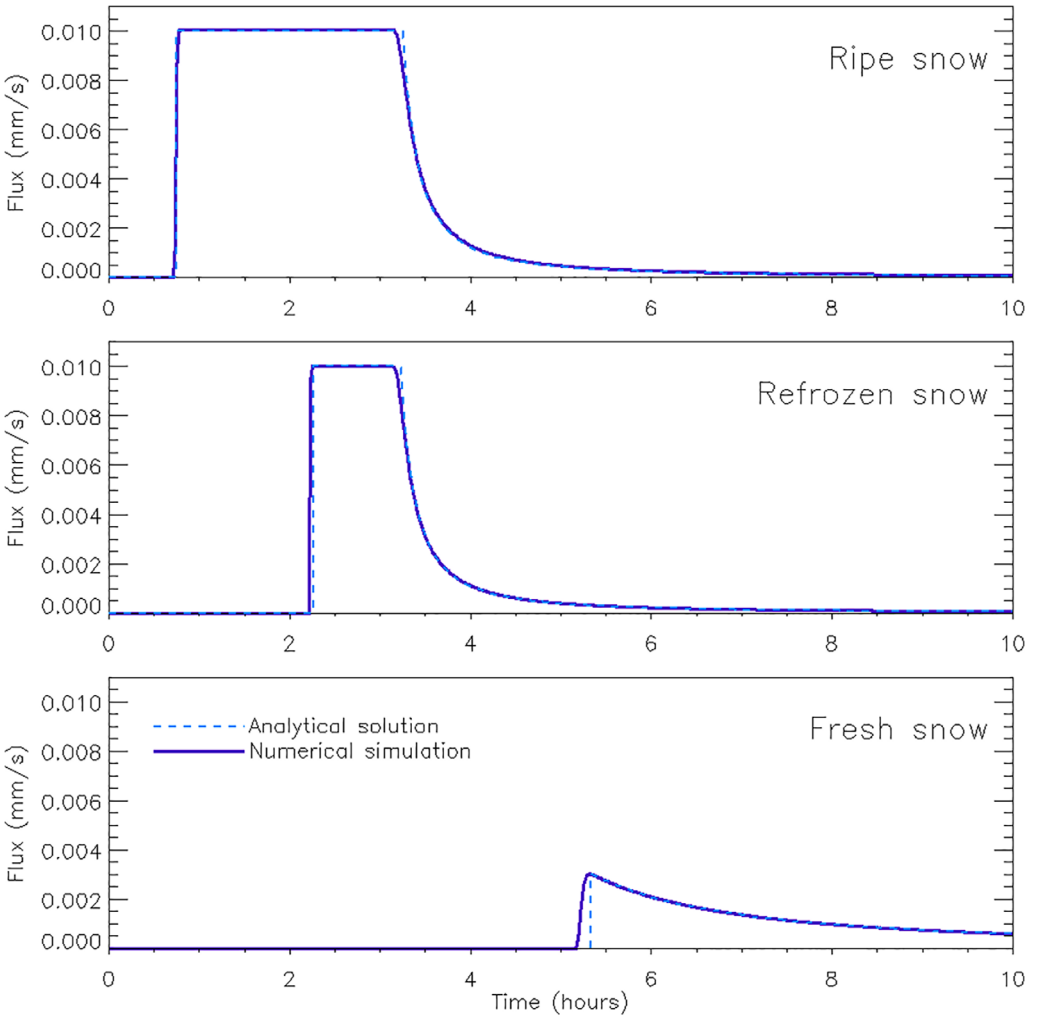

Figure 7. The outflow hydrograph from numerical simulations (solid lines) and analytical solutions (dashed lines), for the ripe snow test case (top plot), the refrozen snow test case (middle plot), and the fresh snow test case (bottom plot),

panel). Because the analytical and numerical solutions depend strictly on gravity driven fluid flow, this indicates numerical diffusion rather than capillary drawing of water ahead of the piston wetting front. The smoothing in the model simulations is most acute in the fresh snow test case, which has much lower permeability than the other test cases (Table 1). Similarly, the outflow hydrographs show close correspondence between model simulations and the analytical solutions, but with an earlier arrival of snowpack outflow in the model simulations of the fresh snow test case.

The numerical model and the analytical solutions use the same equations, and hence the close correspondence between the numerical simulations and the analytical solutions is expected. The more general use of these test cases requires understanding and minimizing differences between a given numerical model and these analytical solutions, and some simplifications/modifications may be required to use these test cases in specific snow models. For example, model modifications may be needed in order to disable the temporal evolution of porosity and grain size (as was done by *Jordan* [1991]). Similarly, model modifications may be needed to ensure that the snow model being tested uses the Brooks-Corey constitutive functions for hydraulic conductivity [*Brooks and Corey*, 1964], as used in equation (7); and model modifications may be needed to disable the capillary term in the unsaturated flow parameterization (if the capillary term is included in the specific snow model being tested). It is also important to recognize simplifications in the analytical solution. The main simplification in the analytical solution presented here is that the water content immediately below the wetting front must be raised to the level of saturation at the wetting

front. This simplification should be considered when interpreting results. We will return to these numerical-analytical differences in the next section.

5. Summary and Discussion

This paper fully develops test cases for the examples of water movement through snow introduced by *Colbeck* [1976]. The work presented here develops general analytical solutions for Colbeck's examples of water movement through snow, and compares the analytical solutions to simulations from a coupled energy and mass balance model. The analytical solutions provide information on both outflow from the snowpack, as well as information on vertical profiles of temperature and volumetric liquid water content at different times throughout the simulation period. Results show that the derived analytical solutions have close correspondence with the numerical model simulations, except for the breakthrough time of the most challenging test.

The discrepancies between the model simulations and the analytical solutions occur for two reasons. First, the spatial discretization and fully implicit time stepping schemes cause some numerical diffusion in the model simulations, resulting in smoother vertical profiles of volumetric liquid water content than the analytical solutions (Figure 6). Second, the model simulations permit flow of water once $\theta_{liq} > \theta_r$, as opposed to the analytical solutions where the downward progression of the wetting front is delayed until $\theta_{liq} > \theta_w$. Hence the numerical simulations produce some snowpack outflow before the true wetting front reaches the bottom of the snowpack.

The intended use of the test cases is to evaluate the impact of different numerical approximations, especially different vertical discretization strategies and different time stepping schemes. Common numerical simplifications in snow models include decoupling the conservation equations for energy and mass, adopting non-iterative numerical solutions for the conservation equations, configuring models with coarse vertical resolution, and ignoring the propagation of water through the snowpack [*Essery et al.*, 2013]. These test cases can hence help to understand accuracy-efficiency tradeoffs in physically motivated models.

Colbeck's examples provide a useful test case for snow models because they evaluate the coupling of hydrology and thermodynamics (i.e., the freezing of water onto the snow grains necessary to supply sufficient latent heat to raise the snow temperature to 0°C), as well as providing a means to evaluate the unsaturated flow of water through porous media. The differences between the ripe snow and refrozen snow cases isolate the coupling of hydrology and thermodynamics, because these cases have the same permeability and different initial temperatures (Table 1). The differences between the refrozen and the fresh snow case isolate the unsaturated flow of water through snow, because these cases have different permeability and the same initial temperature (Table 1). Figures 5 and 7 illustrate the differences among the test cases and the relative controls on permeability and initial temperature.

The test cases developed here have several limitations. First, the test cases are only applicable to gravity-driven flow, and neglect the capillary effects which are now being incorporated in detailed snow models [*Wever et al.*, 2014]. The use of these test cases in these more complex snow models require kinematic simplifications similar to those adopted by *Wigmosta and Lettenmaier* [1999] for saturated subsurface flow. The second limitation is that these test cases are only derived for the Brooks-Corey constitutive functions for hydraulic conductivity [*Brooks and Corey*, 1964], and additional developments are required for alternative closure relationships. Third, the analytical solutions assume that porosity and grain size is constant over the analysis period. Fourth, the constant forcing provides a relatively simple phase change problem. Clearly a broad suite of test cases is required to provide robust evaluation of numerical approximations and the test case presented here represents just one component of a more comprehensive model evaluation strategy.

The motivation for the work presented here is that synthetic test cases are a fundamental (and underutilized) element of any model evaluation strategy. They provide information on the realism of the numerical approximations, and are important to understand how numerical approximations impact the use of models for process evaluation and hypothesis testing. Additional work is required to develop a library of synthetic test cases to discriminate among competing modeling approaches, and to guide model development.

Acknowledgments
This work was supported by the U.S. Army Corps of Engineers. The model simulations in this paper were made using the SUMMA model, which is available at https://www.ral.ucar.edu/projects/summa.

References

Abramowitz, G. (2012), Towards a public, standardized, diagnostic benchmarking system for land surface models, *Geosci. Model Dev.*, *5*, 819–827, doi:10.5194.gmd-5-819-2012.
Abramowitz, G., R. Leuning, M. Clark, and A. Pitman (2008), Evaluating the performance of land surface models, *J. Clim.*, *21*(21), 5468–5481.
Bartelt, P., and M. Lehning (2002), A physical SNOWPACK model for the Swiss avalanche warning. Part I: Numerical model, *Cold Reg. Sci. Technol.*, *35*(3), 123–145, doi:10.1016/s0165-232x(02)00074-5.
Best, M., G. Abramowitz, H. Johnson, A. Pitman, G. Balsamo, A. Boone, M. Cuntz, B. Decharme, P. Dirmeyer, and J. Dong (2015), The plumbing of land surface models: benchmarking model performance, *J. Hydrometeorol.*, *16*(3), 1425–1442.
Beven, K. (1982), On subsurface stormflow: Predictions with simple kinematic theory for saturated and unsaturated flows, *Water Resour. Res.*, *18*(6), 1627–1633.
Boone, A., and P. Etchevers (2001), An intercomparison of three snow schemes of varying complexity coupled to the same land surface model: Local-scale evaluation at an Alpine site, *J. Hydrometeorol.*, *2*(4), 374–394.
Boone, A., and P. J. Wetzel (1996), Issues related to low resolution modeling of soil moisture: Experience with the PLACE model, *Global Planet. Change*, *13*(1-4), 161–181, doi:10.1016/0921-8181(95)00044-5.
Brooks, R. H., and A. T. Corey (1964), Hydraulic properties of porous media and their relation to drainage design, *Trans. Am. Soc. Agric. Eng.*, *7*(1), 26–0028.
Celia, M. A., E. T. Bouloutas, and R. L. Zarba (1990), A general mass-conservative numerical solution for the unsaturated flow equation, *Water Resour. Res.*, *26*(7), 1483–1496, doi:10.1029/90WR00196.
Charbeneau, R. J. (1984), Kinematic models for soil moisture and solute transport, *Water Resour. Res.*, *20*(6), 699–706.
Clark, M. P., and D. Kavetski (2010), Ancient numerical daemons of conceptual hydrological modeling: 1. Fidelity and efficiency of time stepping schemes, *Water Resour. Res.*, *46*, W10511, doi:10.1029/2009WR008894.
Clark, M. P., D. Kavetski, and F. Fenicia (2011), Pursuing the method of multiple working hypotheses for hydrological modeling, *Water Resour. Res.*, *47*, W09301, doi:10.1029/2010WR009827.
Clark, M. P., et al. (2015a), Improving the representation of hydrologic processes in Earth System Models, *Water Resour. Res.*, *51*, 5929–5956, doi:10.1002/2015WR017096.
Clark, M. P., et al. (2015b), A unified approach to process-based hydrologic modeling. Part 1: Modeling concept, *Water Resour. Res.*, *51*, 2498–2514, doi:10.1002/2015WR017198.
Clark, M. P., et al. (2015c), The Structure for Unifying Multiple Modeling Alternatives (SUMMA), version 1: Technical description, NCAR Tech. Note NCAR/TN-514+ STR, 54 pp., Natl. Cent. for Atmos. Res., Boulder, Colo., doi:10.5065/D6WQ01TD.
Clark, M. P., et al. (2015d), A unified approach for process-based hydrologic modeling: Part 2. Model implementation and example applications, *Water Resour. Res.*, *51*, 2515–2542, doi:10.1002/2015WR017200.
Colbeck, S. (1972), A theory of water percolation in snow, *J. Glaciol.*, *11*, 369–385.
Colbeck, S., and E. A. Anderson (1982), The permeability of a melting snow cover, *Water Resour. Res.*, *18*(4), 904–908, doi:10.1029/WR012i003p00523.
Colbeck, S. C. (1976), An analysis of water flow in dry snow, *Water Resour. Res.*, *12*(3), 523–527, doi:10.1029/WR018i004p00904.
Courant, R., and D. Hilbert (1962), *Methods of Mathematical Physics, Volume 2: Differential Equations*, John Wiley, New York.
Desborough, C. (1999), Surface energy balance complexity in GCM land surface models, *Clim. Dyn*, *15*(5), 389–403.
Essery, R., S. Morin, Y. Lejeune, and C. B. Menard (2013), A comparison of 1701 snow models using observations from an alpine site, *Adv. Water Resour.*, *55*, 131–148, doi:10.1016/j.advwatres.2012.07.013.
Hansson, K., J. Simunek, M. Mizoguchi, L. C. Lundin, and M. T. van Genuchten (2004), Water flow and heat transport in frozen soil: Numerical solution and freeze-thaw applications, *Vadose Zone J.*, *3*(2), 693–704.
Hogue, T. S., L. A. Bastidas, H. V. Gupta, and S. Sorooshian (2006), Evaluating model performance and parameter behavior for varying levels of land surface model complexity, *Water Resour. Res.*, *42*, W08430, doi:10.1029/2005WR004440.
Jakeman, A., and G. Hornberger (1993), How much complexity is warranted in a rainfall-runoff model?, *Water Resour. Res.*, *29*(8), 2637–2649.
Jordan, R. (1991), A One-Dimensional Temperature Model for a Snow Cover: Technical Documentation for SNTHERM.89, 49 pp., U.S. Army Corps of Eng., Hanover, N. H.
Kavetski, D., and M. P. Clark (2010), Ancient numerical daemons of conceptual hydrological modeling: 2. Impact of time stepping schemes on model analysis and prediction, *Water Resour. Res.*, *46*, W10511, doi:10.1029/2009WR008896.
Kavetski, D., and M. P. Clark (2011), Numerical troubles in conceptual hydrology: Approximations, absurdities and impact on hypothesis testing, *Hydrol. Processes*, *25*(4), 661–670, doi:10.1002/hyp.7899.
Kurylyk, B. L., J. M. McKenzie, K. T. MacQuarrie, and C. I. Voss (2014), Analytical solutions for benchmarking cold regions subsurface water flow and energy transport models: One-dimensional soil thaw with conduction and advection, *Adv. Water Resour.*, *70*, 172–184.
Lawrence, D. M., et al. (2011), Parameterization improvements and functional and structural advances in Version 4 of the Community Land Model, *J. Adv. Model. Earth Syst.*, *3*, M03001, doi:10.1029/2011MS000045.
Luce, C. H., and T. W. Cundy (1992), Modification of the Kinematic Wave—Philip Infiltration Overland Flow Model, *Water Resour. Res.*, *28*(4), 1179–1186.
Luce, C. H., D. G. Tarboton, and K. R. Cooley (1999), Sub-grid parameterization of snow distribution for an energy and mass balance snow cover model, *Hydrol. Processes*, *13*(12-13), 1921–1933, doi:10.1002/(sici)1099-1085(199909)13:12/13 < 1921::aid-hyp867 > 3.3.co;2-j.
Magnusson, J., N. Wever, R. Essery, N. Helbig, A. Winstral, and T. Jonas (2015), Evaluating snow models with varying process representations for hydrological applications, *Water Resour. Res.*, *51*, 2707–2723, doi:10.1002/2014WR016498.
Marks, D., J. Domingo, D. Susong, T. Link, and D. Garen (1999), A spatially distributed energy balance snowmelt model for application in mountain basins, *Hydrol. Processes*, *13*(1213), 1935–1959.
Maxwell, R. M., M. Putti, S. Meyerhoff, J. O. Delfs, I. M. Ferguson, V. Ivanov, J. Kim, O. Kolditz, S. J. Kollet, and M. Kumar (2014), Surface-subsurface model intercomparison: A first set of benchmark results to diagnose integrated hydrology and feedbacks, *Water Resour. Res.*, *50*, 1531–1549, doi:10.1002/2013WR013725.
Nearing, G. S., D. M. Mocko, C. D. Peters-Lidard, S. V. Kumar, and Y. Xia (2016), Benchmarking NLDAS-2 soil moisture and evapotranspiration to separate uncertainty contributions, *J. Hydrometeorol.*, *17*(3), 745–759.
Niu, G. Y., et al. (2011), The community Noah land surface model with multiparameterization options (Noah-MP): 1. Model description and evaluation with local-scale measurements, *J. Geophys. Res.*, *116*, D12109, doi:10.1029/2010JD015139.
Shimizu, H., (1970), Air permeability of deposited snow, *Contrib. Inst. Low Temp. Sci., Ser. A*, *22*, 1–32.
Sisson, J., A. Ferguson, and M. T. Van Genuchten (1980), Simple method for predicting drainage from field plots, *Soil Sci. Soc. Am. J.*, *44*(6), 1147–1152.

Stöckli, R., D. Lawrence, G. Y. Niu, K. Oleson, P. Thornton, Z. L. Yang, G. Bonan, A. Denning, and S. Running (2008), Use of FLUXNET in the Community Land Model development, *J. Geophys. Res.*, *113*, G01025, doi:10.1029/2007JG000562.

Vionnet, V., E. Brun, S. Morin, A. Boone, S. Faroux, P. Le Moigne, E. Martin, and J. Willemet (2012), The detailed snowpack scheme Crocus and its implementation in SURFEX v7.2, *Geosci. Model Dev.*, *5*, 773–791.

Wever, N., C. Fierz, C. Mitterer, H. Hirashima, and M. Lehning (2014), Solving Richards Equation for snow improves snowpack meltwater runoff estimations in detailed multi-layer snowpack model, *Cryosphere*, *8*(1), 257–274.

Wigmosta, M. S., and D. P. Lettenmaier (1999), A comparison of simplified methods for routing topographically driven subsurface flow, *Water Resour. Res.*, *35*(1), 255–264, doi:10.1029/1998WR900017.

Yang, Z. L., et al. (2011), The community Noah land surface model with multiparameterization options (Noah-MP): 2. Evaluation over global river basins, *J. Geophys. Res.*, *116*, D12110, doi:10.1029/2010JD015140.

Yilmaz, K. K., H. V. Gupta, and T. Wagener (2008), A process-based diagnostic approach to model evaluation: Application to the NWS distributed hydrologic model, *Water Resour. Res.*, *44*, W09417, doi:10.1029/2007WR006716.